IEEE Photonics Journal
An IEEE Photonics Society Publication

Compact Single-Mode Silicon Hybrid Rib/Strip Waveguide With Adiabatic Bends

Volume 3, Number 3, June 2011

W. Bogaerts, Member, IEEE
S. K. Selvaraja, Student Member, IEEE

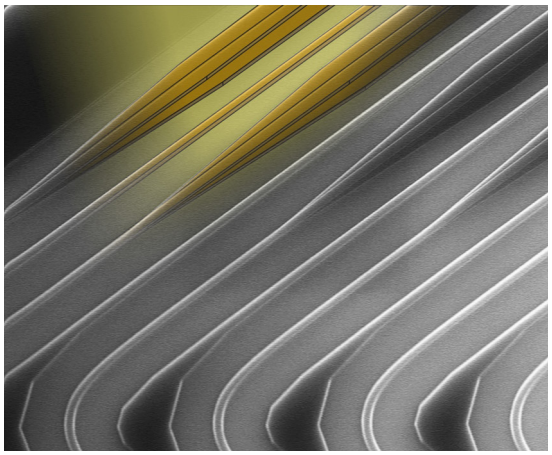

DOI: 10.1109/JPHOT.2011.2142931
1943-0655/$26.00 ©2011 IEEE

IEEE photonics SOCIETY

IEEE

Compact Single-Mode Silicon Hybrid Rib/Strip Waveguide With Adiabatic Bends

W. Bogaerts, *Member, IEEE*, and S. K. Selvaraja, *Student Member, IEEE*

Ghent University—IMEC, Department of Information Technology,
Photonics Research Group, 9000 Gent, Belgium

DOI: 10.1109/JPHOT.2010.2142931
1943-0655/$26.00 ©2011 IEEE

Manuscript received March 11, 2011; revised April 6, 2011; accepted April 6, 2011. Date of publication April 21, 2011; date of current version May 6, 2011. This work was supported in part by the European Union through the FP7-ICT-HELIOS project. W. Bogaerts acknowledges the Flemish Research Foundation (FWO-Vlaanderen) for a postdoctoral fellowship. Corresponding author: W. Bogaerts (e-mail: wim.bogaerts@intec.ugent.be).

Abstract: We report a low-loss, hybrid silicon waveguide geometry that consists of straight rib sections with a propagation loss of 0.27 ± 0.012 dB/cm and compact photonic wire bends. The rib and wire waveguides are both single mode and connected through a short double-etched linear taper section. To reduce bend losses, circular bends were combined with variable adiabatic seminatural spline shapes with only a limited footprint penalty.

Index Terms: Silicon photonics, waveguides, bends.

1. Introduction

Silicon photonic circuits are coming of age, with the first applications appearing on the market. The main advantage of using silicon for photonics is that it is possible to use the existing complementary metal–oxide semiconductor (CMOS) manufacturing infrastructure [1], [2], while at the same time having a material system that is both transparent at telecom wavelengths and provides a high index contrast. The large contrast enables shrinking waveguides to submicrometer dimensions that still have a large confinement of light in the core. However, the large index contrast comes with a significant drawback: Scattering losses are much higher [3], [4]. Also, the small-core waveguides are also much more sensitive to small dimensional variations, which can introduce phase errors in the long waveguides [5], [6]. The combination of both effects makes it difficult to make long delay lines in silicon.

The high contrast of silicon also enables tight bends. However, as in any waveguide system, the transition between a straight waveguide and a circular bend gives rise to a mode mismatch, as the peak of the bend mode is shifted slightly to the outside of the bend. One of the traditional ways is to compensate this by introducing an offset, shifting the centerline of the bent waveguide slightly to the center of the bend, compared with the centerline of the straight waveguide [7]–[9]. However, with silicon photonic wire waveguides, this is quite difficult, as the offset is typically of the order of nanometers, which is often smaller than the fabrication grid. Alternatively, one can use cosine bends, which are typically used for S-bend connections but can be generalized [10]. Spline bends have been proposed as an alternative to a circular bend with a lower loss [11], but this method brings only limited improvement because it is constrained to the same footprint. Koos *et al.* proposed a method for analytically optimizing the entire bend shape to minimize losses [12], but this method requires reoptimization for different bend angles and radius.

We present an alternative solution to adiabatically transform the straight waveguide into a circular bend by introducing a small spline section at the straight–bend interface. In Section 2, we construct

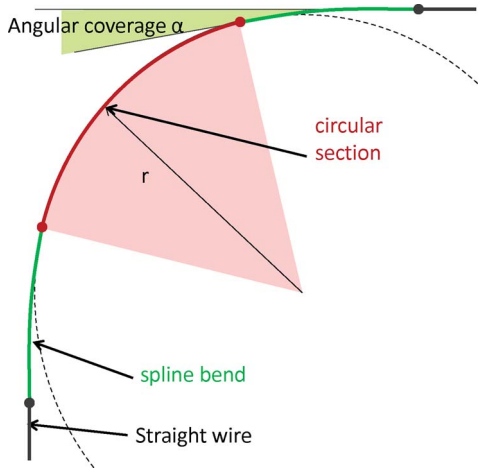

Fig. 1. Bend design using a spline transition between the straight section and the bend section. The curvature is matched at both ends of the spline, which covers an angle α of the entire bend.

the spline sections based on the minimal bend radius, and we discuss the penalties this will introduce in terms of footprint. We will experimentally demonstrate that the spline bends significantly outperform circular bends with a larger bend radius.

Overall propagation losses are also one of the main limitations of silicon photonic wires. The best stepper-fabricated monocrystalline silicon wires demonstrated have losses larger than 2 dB/cm [2], [13], [14], and with e-beam fabrication, it is 1 dB/cm [15]. Etched wire waveguide are the most versatile to design integrated components such as ring resonators. Any additional postprocessing to reduce sidewall roughness (e.g., oxidation) can complicate the design. However, to mitigate the propagation losses of such photonic wires, we can combine them with lower loss waveguides. It has been shown that low-loss ($\sim$0.3 dB/cm) waveguide circuits can be achieved by multimode straight and single-mode bends [16]. However, the expansion in mode size requires a taper that is over 150 μm in length. Also, any mode mixing in the multimode section will translate into additional losses. Alternatively, one can switch from a wire waveguide to a shallow-etched or partially oxidized rib waveguide: The propagation loss can be significantly reduced by reducing the overlap between the waveguide mode and the sidewall, while still keeping the mode size quite small. However, the smaller lateral index contrast makes small microbends difficult [17]–[19]. We combine both techniques by employing a shallow-etched, single-mode rib waveguide in the straight sections and a single-mode wire in the bends. We show in Section 3 that this significantly reduces the overall propagation losses, again with a relatively small penalty in footprint.

The advantage of these designs is that that they can be applied on top of any process optimization, such as sidewall passivation or improved lithography or etch chemistry.

2. Adiabatic Bends

The interface between a straight waveguide and a circular bend must be engineered to minimize reflections and losses due to an abrupt mode mismatch [7]–[10]. For this, we propose a spline based transition section, as illustrated in Fig. 1. Between the straight waveguide and the circular bend section, we introduce a polynomial spline which at both ends matches the curvature of the adjacent waveguide. As we have four boundary conditions (one positional coordinate and the curvature at each end point), we can always find a solution with a third-order (cubic) spline.

In principle, we could construct the entire bend from a natural spline [20], as a natural spline has zero curvature at both ends. However, a natural spline with a given minimal bend radius is also much larger than a circular bend with the same radius. For a 90° bend, the characteristic spline length L is almost three times larger than the minimal bend radius r_{min}

$$r_{\text{min}} = 0.27L. \tag{1}$$

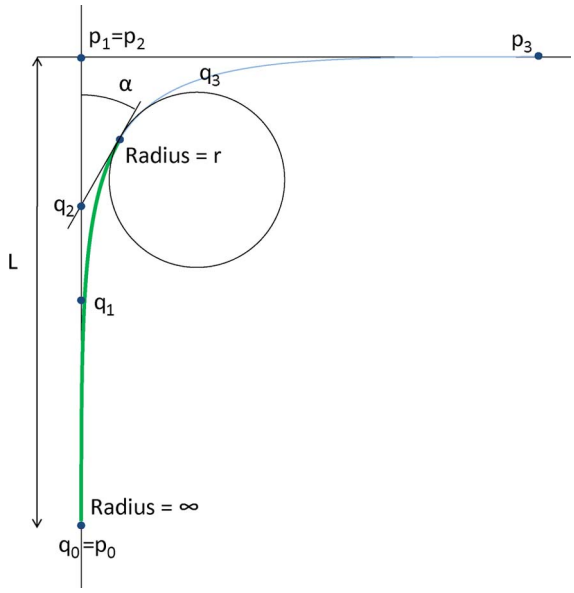

Fig. 2. Construction of a partial half-natural spline from the full natural spline for a 90° bend.

Therefore, to reduce the footprint of the bend, we only cover a part of the bend angle using a spline. This is indicated in Fig. 1 by the angular coverage α. For $\alpha = 0°$ we get a circular bend, while for $\alpha = 45°$, we get the complete natural spline.

2.1. Construction of the Spline Section

Knowing that we need to have a zero curvature at one end, we can characterize the spline section by only two parameters: the minimal radius r at the other end and the coverage angle α. There are several ways to construct the spline section, but we start from the full natural cubic spline which covers the entire bend, as shown in Fig. 2. Such a spline can be defined as a Bezier curve with four control points q_i, with $i = 0, \ldots, 3$ [21]. For a natural spline, which has zero curvature in both end points, q_1 and q_2 coincide. For the ease of calculation, we take that point as the origin. The two other control points coincide with the end points of the curve, which, for a natural spline covering a 90° angle, are located at $(L, 0)$ and $(0, L)$. L is the characteristic length of the natural spline.

If we want to cover the entire 90° bend with a spline shape, we would now only need to scale the spline to match the desired minimum bend radius. However, if we want to cover only a partial angle α with a spline and the rest with a simple circular bend, we need some additional calculations. First, we need to calculate the position along the natural spline with a slope which corresponds to the angle α. As we express our spline in term of Bezier control points, we calculate the interval-parameter t_0 (with $t \in [0, 1]$) of the Bezier curve [22]. We find that

$$t_\alpha = \sin^2\left(\arctan\sqrt[4]{\cot\alpha}\right). \tag{2}$$

Only now we can set the characteristic length of the natural spline, as we need to scale it to the radius in the point corresponding with t_α

$$L = 2r\frac{t_\alpha(1 - t_\alpha)}{3\sqrt{t_\alpha^4 + (1 - t_\alpha)^4}^3}. \tag{3}$$

Based on this characteristic length, we can define the actual control points p_i of the complete natural spline. From those control points, we can now calculate the control points q_i of the partial

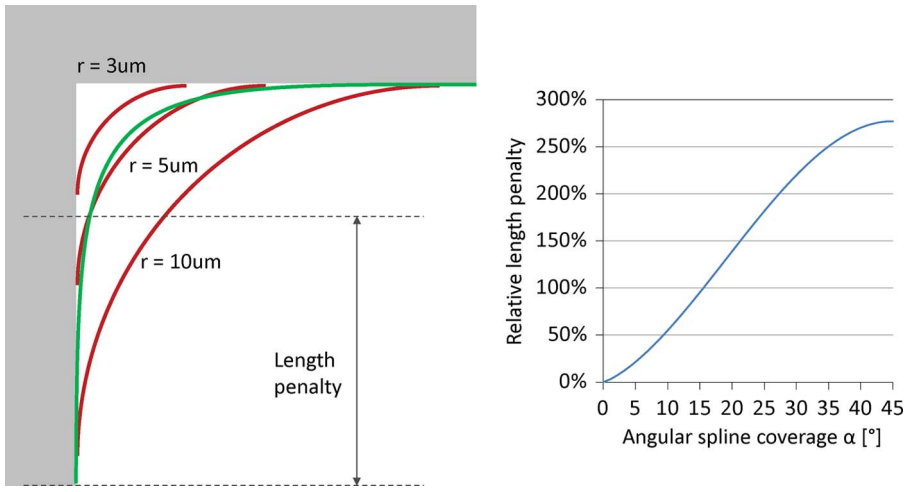

Fig. 3. Bend side length penalty for different angular coverage of the spline section. (Left) Spline bend with 3 μm minimum radius, compared with circular bends of 3, 5, and 10 μm radius. (Right) Relative length penalty as function of spline angle coverage.

spline, using the Casteljau algorithm [22]

$$\begin{aligned} q_0 &= p_0 \\ q_1 &= t_\alpha p_0 + (1 - t_\alpha) p_1 \\ q_2 &= t_\alpha^2 p_0 + 2t_\alpha (1 - t_\alpha) p_1 + (1 - t_\alpha)^2 p_2 \\ q_3 &= t_\alpha^3 p_0 + 3t_\alpha^2 (1 - t_\alpha) p_1 + 3t_\alpha (1 - t_\alpha)^2 p_2 + (1 - t_\alpha)^3 p_3. \end{aligned} \tag{4}$$

We can now use these control points to generate a Bezier curve for the spline part of our bend. However, we still have to translate the Spline part to interface it at the correct point of the circular bend. For bends at different angles, we can perform (4) but on a different set of control points for the full natural spline.

Finally, the design was implemented as a mask layout using our Python-driven parametric design framework IPKISS [23], [24], using a grid-limited Casteljau algorithm [22]. The waveguides are generated from a set of control points at the bend vertices, and the mask layout is automatically generated.

2.2. Penalty in Footprint

A bend with spline sections will be larger than a circular bend with the same radius. We already say that the characteristic length of the complete natural spline bend is almost four times larger than that of the circular bend. Still, the actual penalty is much less when using a partial spline bend. We discuss two metrics to assess the footprint penalty of the spline bend.

The most straightforward way of measuring the bend size is through its edge length. This is illustrated in Fig. 3. If a bend needs to fill the inside of a corner, we find that the spline section adds somewhat in length to the circular bend, which increases with the angular coverage α. For small α, the penalty is modest, but a complete natural spline $(\alpha = 45^\circ)$ with a 3 μm bend radius consumes more length than a 10 μm bend.

However, this penalty metric is not necessarily representative. A better penalty metric is shown in Fig. 4. Bends are usually used to route around objects and have to keep a certain distance. If we keep this minimum offset in the corner, we can now calculate the additional offset introduced by the spline section. We see that this penalty is much less severe, staying under 20% of the bend radius, even for the complete spline bend.

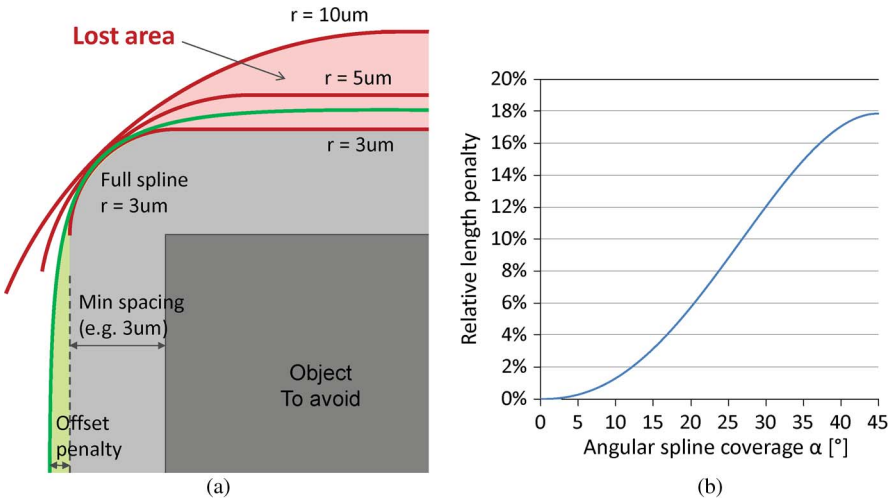

Fig. 4. Bend offset penalty for different angular coverage of the spline section. (a) Spline bend with 3 μm minimum radius compared with circular bends of 3, 5 and 10 μm radius. (b) Relative offset penalty as function of spline angle coverage.

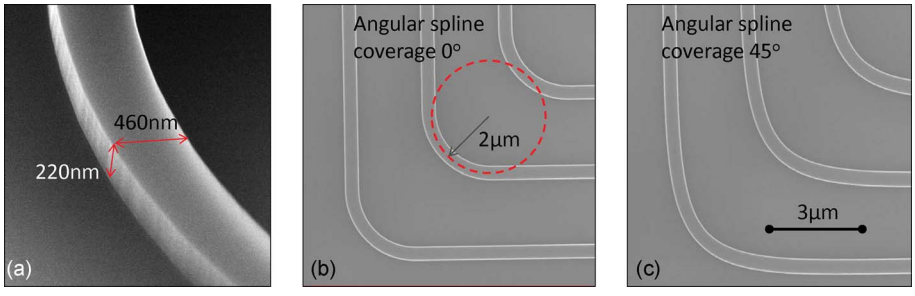

Fig. 5. (a) SEM picture of a photonic wire waveguide. (b) Top view of a circular bend with 2 μm bend radius and a (c) complete spline bend with the same minimal bend radius.

2.3. Fabrication

The waveguides were fabricated in the *imec* 200 mm CMOS pilot line, using silicon-on-insulator wafers with 220 nm of silicon and 2 μm buried oxide. The patterns were lithographically defined in a 330 nm of photoresist using a PAS5500/1100 scanner operating at 193 nm wavelength. After lithography, the pattern is transferred using Inductive Coupled Plasma-Reactive Ion Etch (ICP-RIE) etching with a chlorine/bromine chemistry [14]. After patterning, a top cladding of silicon dioxide is deposited using plasma deposition. No additional postprocessing (e.g., sidewall oxidation, chemical passivation) was done. An image of a photonic wire waveguide prior to oxide deposition is shown in Fig. 5(a).

2.4. Measurements

To characterize the waveguide losses, we measured the transmission through several spirals with different lengths. The spirals consisted entirely of photonic wires with a width of 460 nm. Light is coupled into the chips using vertical grating couplers [25], [26] with a coupling efficiency of 31% for the transverse electric-polarized mode at 1550 nm wavelength. For each spiral, the transmitted power was optimized, and a spectrum was collected using a broadband light source and an optical spectrum analyzer.

Fig. 6 shows the straight propagation losses extracted from four spirals of 1, 2, 4, and 7 cm length. For the radius, we choose a safe 10 μm bend radius, for which we have found that the excess bend loss (compared with a straight waveguide with the same length) is negligible. We find that the overall losses are quite low: between 1.2 and 1.5 dB/cm over the measurement interval.

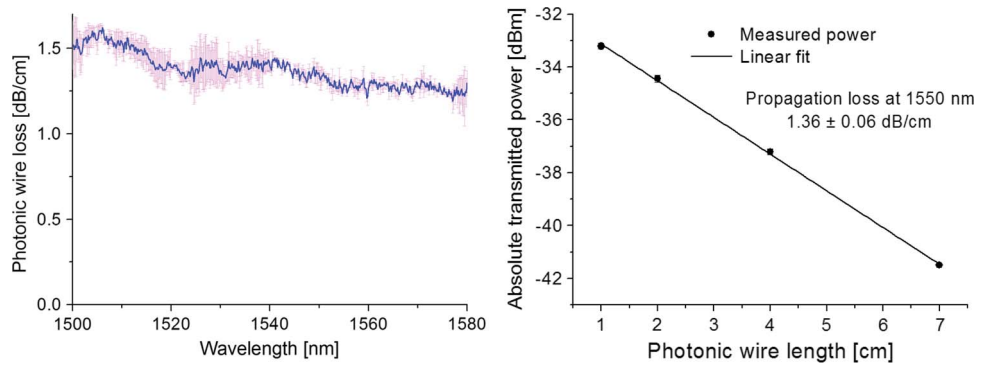

Fig. 6. Propagation loss [dB/cm] of a photonic wire of 460 nm wide and 220 nm high. (Left) Loss as function of wavelength. (Right) Measured power for different spiral lengths at 1550 nm.

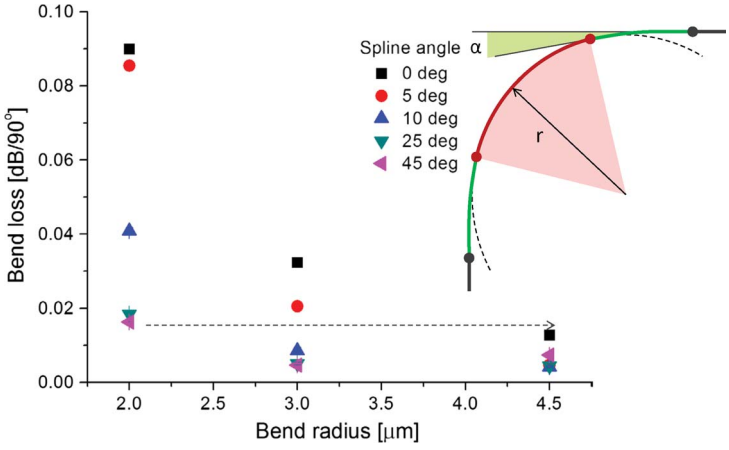

Fig. 7. Bend loss of photonic wires (460 nm $\times$ 220 nm) with 2–4.5 μm bend radius for different spline angles.

In a similar way, we measured the losses of the spline bends. Only now, we used a set of spirals with the same length of 2.3 cm but with the number of bends increasing from 18 to 387. We did this for bends with a minimal radius of 2, 3, and 4.5 μm and with angular coverage α of 0°, 5°, 10°, 25°, and 45° (full spline). The difference between a circular bend with 2 μm radius and a complete spline bend with the same radius is illustrated in the scanning electron microscope pictures in Fig. 5(b) and (c). The extracted bend loss is plotted in Fig. 7. We see that the spline section introduces a significant reduction of the bend losses, especially for smaller bends. A 2 μm full spline bend has about the same loss as a 4.5 μm circular bend, with a larger length penalty but a much lower offset penalty. We also see that the most improvement comes from the first 10° of angular coverage. Unless it is for very small bends, it is therefore not necessary to use the full spline, and most of the bend can be circular.

3. Hybrid Rib/Wire Waveguide

3.1. Design

Still, even with losses close to 1 dB/cm, the usable line length of a photonic wire waveguide is limited. A shallow-etched rib waveguide has much less sidewall surface and modal overlap with the patterning-induced roughness. However, a shallow-etched rib waveguide is laterally surrounded by

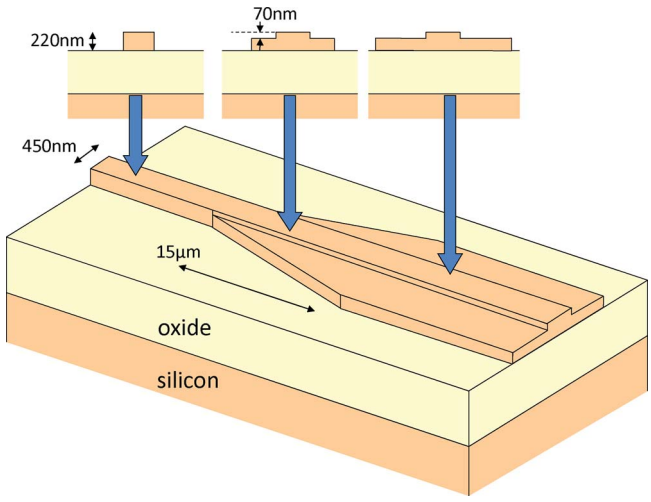

Fig. 8. Transition between a wire and rib waveguides using a double linear taper.

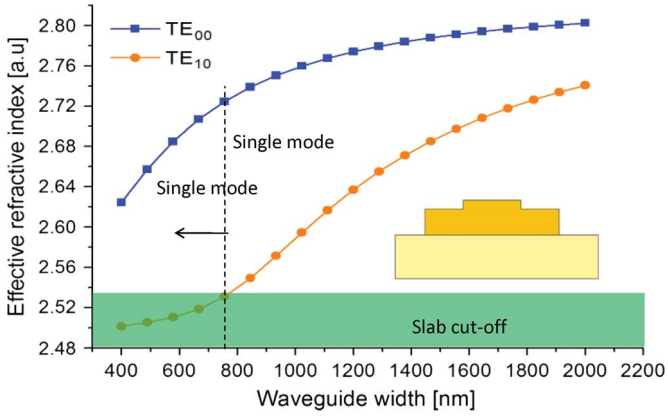

Fig. 9. Guided rib modes as a function of rib width at 1550 nm wavelength. Below 750 nm the rib is single mode.

a thinner silicon slab and, therefore, has much less confinement. This increases the bend losses, and sharp bends are no longer possible. A good solution is to use a photonic wire waveguide where bends are needed and only use the rib waveguide in the straight sections.

Fig. 8 sketches the transition between the rib and the wire waveguide, using a double linear taper section. We used a 15 μm taper, but we have already used similar taper sections as short as 3 μm [5], [6] and even parabolic taper sections [27]. We expand the 460 nm wire to a 700 nm wide rib waveguide. Both waveguides are still single mode, as can be seen from Fig. 9.

We implemented the complete hybrid rib/wire waveguide in the IPKISS design framework and included the spline bend shape for the wire bend. This is shown in Fig. 10.

3.2. Fabrication

For the hybrid rib/wire waveguide, we used two different mask layers: one to define the rib waveguides and one to define the wire waveguides (see Fig. 11). First the shallow-etched structures were defined, including the grating fiber couplers, which are used for characterization. For this, 70 nm of silicon is etched by using an ICP-RIE process. Next, the photonic wire structures are

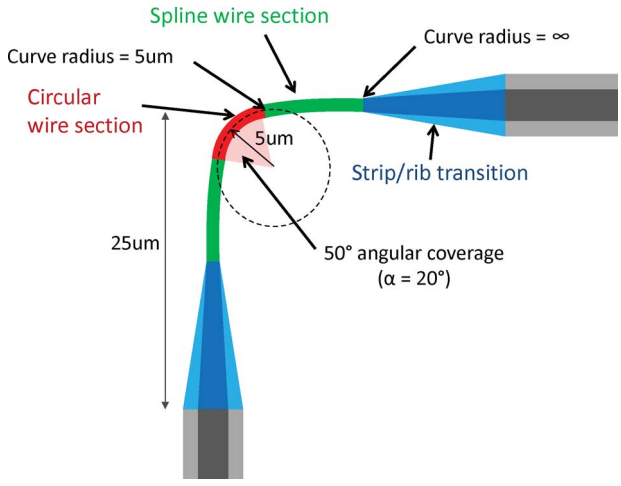

Fig. 10. Design of a hybrid bend with rib/wire transitions and spline sections in the photonic wire.

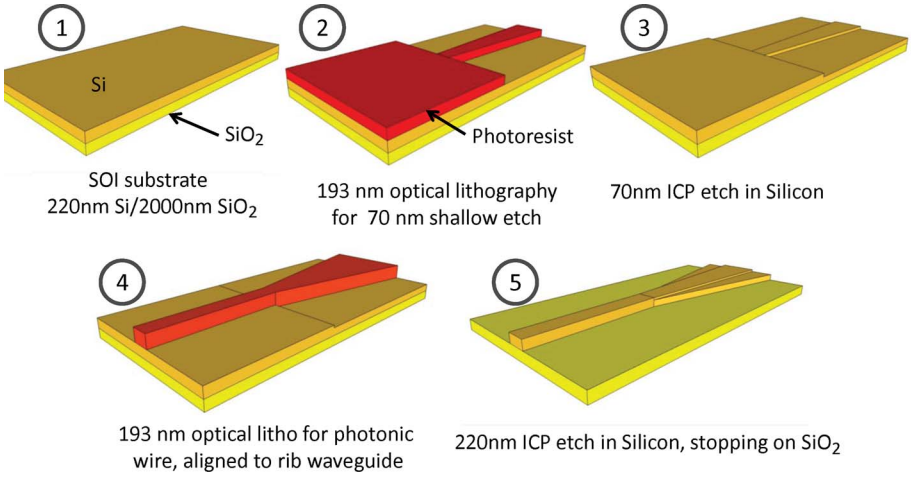

Fig. 11. Fabrication of the rib/wire transition using two etch steps.

lithographically aligned to the previously defined shallow-etched structure. High alignment accuracy ($<$ 12 nm) of the 193 nm optical scanner allows good alignment between the two layers, which is crucial to avoiding the mode mismatch between the shallow rib waveguide and photonic wire bends [6], [14]. During optical lithography, the exposure dose for the waveguides was swept from east to west over the wafer, resulting in varying waveguide widths for the deep-etched wires. The shallow-etched structures were not varied. The resulting structure is shown in Fig. 12.

3.3. Measurements

Losses were characterized using a set of nine spirals, where the straight sections of the spirals have the rib waveguide geometry. To differentiate between the losses in the straight sections (due to the rib waveguides) and the losses in the bends (due to the bend, as well as the transitions), we varied the total length between 4 and 16 cm and the number of bends between 34 and 456. This gives us a 2-D parameter space where we can extract the separate contributions through a bilinear fit. The spline angular coverage α was fixed at 20°. This is illustrated in Fig. 13.

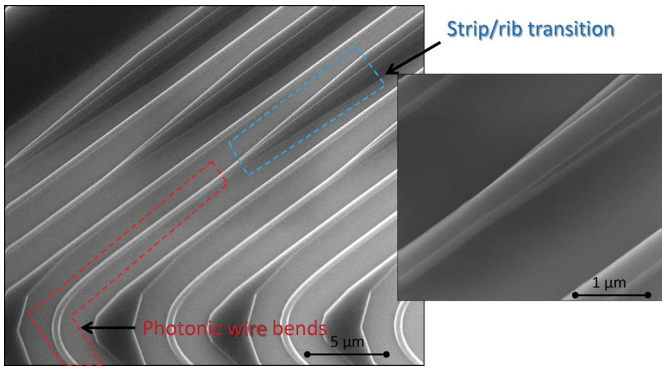

Fig. 12. SEM picture of the fabricated rib/wire waveguide with a transition and a spline bend before oxide cladding deposition.

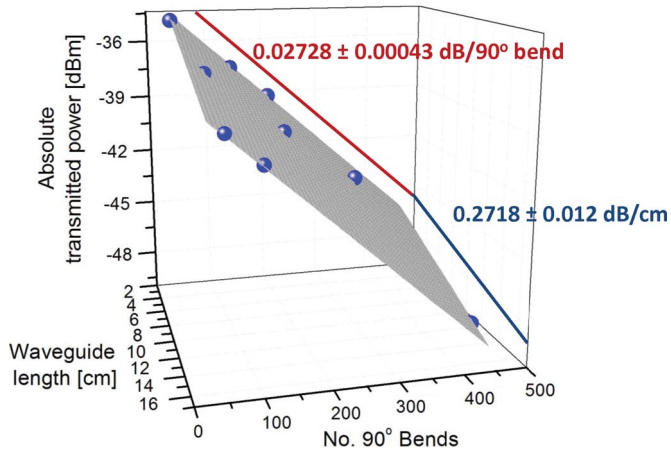

Fig. 13. Propagation loss and bend loss extraction from the fitting a 2-D plane.

TABLE 1

Propagation loss and bend loss of 700 nm wide rib waveguide with wire bends

Wire width [nm]	Rib waveguide loss [dB/cm]	Total bend loss [dB/90°]
470	0.271 ± 0.012	0.027 ± 0.004
460	0.286 ± 0.019	0.032 ± 0.001
420	0.33 ± 0.05	0.068 ± 0.002

For the straight sections, we find a rib waveguide propagation loss of 0.2718 $\pm$ 0.012 dB/cm and a bend loss of 0.0273 $\pm$ 0004 dB per 90° bend, including the two transitions between a rib and a wire. If we consult Fig. 7, we can estimate the loss contribution of a spline bend with $\alpha = 20°$ and a radius $r = 5$ μm to be 0.004 dB. This gives a residual loss of 0.012 dB per rib/wire transition.

As we varied the wire width over the wafers by changing the lithographic exposure dose for the deep etch, we can also look at the influence of waveguide width on the bend loss. This is shown in Table 1. As we would expect, the losses of the rib waveguide vary only slightly, as its dimensions were not changed, but the bend losses increase dramatically when the waveguide is narrower. This can be attributed to both lower confinement (and thus larger bend radiation losses) and increased overlap with the sidewall (more scattering losses at sidewall roughness).

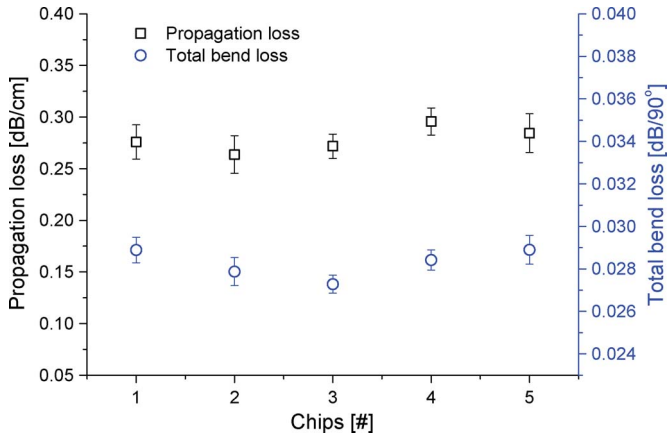

Fig. 14. Measured propagation loss and bend loss for the hybrid rib/strip waveguide for different chips over a 200 mm wafer. The total bend loss incorporates the transition from a rib waveguide to a wire, a spline bend of 90°, and a second transition back to a rib waveguide.

We also measured five nominally identical chips from the same wafer, and the propagation loss at 1550 nm is shown in Fig. 14. We observe a wafer-level variation of only 0.016 dB/cm for the propagation loss of the rib sections and 0.001 dB/90° for the total bend loss. These variations are below the measurement error, which suggests that the such low-loss waveguides can be fabricated reliably over a 200 mm wafer in a CMOS pilot line.

4. Conclusion

We have designed and fabricated a hybrid silicon rib/wire waveguide with significantly lower propagation losses compared with simple photonic wire waveguide. Compared with monocrystalline silicon wires of 460 nm × 220 nm, losses in the straight rib sections decrease from 1.36 dB/cm to about 0.27 dB/cm. For the bend sections, photonic wires can be used by using a double linear taper transition section between the rib and the wire. To reduce the bend losses, we introduced a natural spline section to make a gradual change in bend curvature. This results in a dramatic reduction in bend loss, with only a small footprint penalty. For example, for a 3 μm bend radius, the use of a 10° spline section reduced the excess bend loss from 0.037 dB to 0.009 dB. These design improvements can be applied on top of process optimizations such as improved etch recipes or sidewall passivation.

Acknowledgment

The authors acknowledge the ePIXfab MPW and the *imec* pilot line for the fabrication of their devices.

References

[1] C. Gunn, "CMOS photonics for high-speed interconnects," *IEEE Micro*, vol. 26, no. 2, pp. 58–66, Mar./Apr. 2006.
[2] W. Bogaerts, R. Baets, P. Dumon, V. Wiaux, S. Beckx, D. Taillaert, B. Luyssaert, J. Van Campenhout, P. Bienstman, and D. Van Thourhout, "Nanophotonic waveguides in Silicon-on-insulator fabricated with CMOS technology," *J. Lightwave Technol.*, vol. 23, no. 1, pp. 401–412, Jan. 2005.
[3] S. Johnson, M. Povinelli, M. Soljacic, A. Karalis, S. Jacobs, and J. Joannopoulos, "Roughness losses and volume-current methods in photonic-crystal waveguides," *Appl. Phys. B*, vol. 81, no. 2/3, pp. 283–293, Jul. 2005.
[4] W. Bogaerts, P. Bienstman, and R. Baets, "Scattering at sidewall roughness in photonic crystal slabs," *Opt. Lett.*, vol. 28, no. 9, pp. 689–691, May 2003.
[5] W. Bogaerts, P. Dumon, D. Van Thourhout, D. Taillaert, P. Jaenen, J. Wouters, S. Beckx, V. Wiaux, and R. Baets, "Compact wavelength-selective functions in silicon-on-insulator photonic wires," *J. Sel. Top. Quantum Electron.*, vol. 12, no. 6, pp. 1394–1401, Dec. 2006.

[6] W. Bogaerts, S. Selvaraja, P. Dumon, J. Brouckaert, K. De Vos, D. Van Thourhout, and R. Baets, "Silicon-on-insulator spectral filters fabricated with CMOS technology," *IEEE J. Sel. Topics Quantum Electron.*, vol. 16, no. 1, pp. 33–44, Jan./Feb. 2010.
[7] S. Kim and A. Gopinath, "Vector analysis of optical dielectric waveguide bends using finite-difference method," *J. Lightwave Technol.*, vol. 14, no. 9, pp. 2085–2092, Sep. 1996.
[8] L. Spiekman, Y. Oei, E. Metaal, F. Groen, P. Demeester, and M. Smit, "Ultrasmall waveguide bends: The corner mirrors of the future?" *Proc. Inst. Elect. Eng.—Optoelectron.*, vol. 142, no. 1, pp. 61–65, Feb. 1995.
[9] M. Smit, E. Pennings, and H. Blok, "A normalized approach to the design of low-loss optical waveguide bends," *J. Lightw. Technol.*, vol. 11, no. 11, pp. 1737–1742, Nov. 1993.
[10] F. Mustieles, E. Ballesteros, and P. Baquero, "Theoretical s-bend profile for optimization of optical waveguide radiation losses," *IEEE Photon. Technol. Lett.*, vol. 5, no. 5, pp. 551–553, May 1993.
[11] Z. Hu and Y. Lu, "Computing optimal waveguide bends with constant width," *J. Lightwave Technol.*, vol. 25, no. 10, pp. 3161–3167, Oct. 2007.
[12] C. Koos, C. G. Poulton, L. Zimmermann, L. Jacome, J. Leuthold, and W. Freude, "Ideal bend contour trajectories for single-mode operation of low-loss overmoded waveguides," *IEEE Photon. Technol. Lett.*, vol. 19, no. 11, pp. 819–821, Jun. 2007.
[13] Y. A. Vlasov and S. McNab, "Losses in single-mode silicon-on-insulator strip waveguides and bends," *Opt. Express*, vol. 12, no. 8, pp. 1622–1631, Apr. 2004.
[14] S. Selvaraja, P. Jaenen, W. Bogaerts, D. Van Thourhout, P. Dumon, and R. Baets, "Fabrication of photonic wire and crystal circuits in silicon-on-insulator using 193 nm optical lithography," *J. Lightwave Technol.*, vol. 27, no. 18, pp. 4076–4083, Sep. 2009.
[15] M. Gnan, S. Thoms, D. Macintyre, R. De La Rue, and M. Sorel, "Fabrication of low-loss photonic wires in silicon-on-insulator using hydrogen silsesquioxane electron-beam resist," *Electron. Lett.*, vol. 44, no. 2, pp. 115–116, Jan. 2008.
[16] S. Spector, M. W. Geis, D. Lennon, R. C. Williamson, and T. Lyszczarz, "Hybrid multi-mode/single-mode waveguides for low loss," in *Optical Amplifiers and Their Applications/Integrated Photonics Research*. San Francisco, CA: Opt. Soc. Amer., 2004, p. IThE5. [Online]. Available: http://www.opticsinfobase.org/abstract.cfm?URI=IPR-2004-IThE5
[17] M. Webster, R. Pafchek, G. Sukumaran, and T. Koch, "Low-loss quasi-planar ridge waveguides formed on thin silicon-on-insulator," *Appl. Phys. Lett.*, vol. 87, no. 23, p. 231 108, Dec. 5, 2005.
[18] L. K. Rowe, M. Elsey, N. G. Tarr, A. P. Knights, and E. Post, "CMOS-compatible optical rib waveguides defined by local oxidation of silicon," *Electron. Lett.*, vol. 43, no. 7, pp. 392–393, Mar. 29, 2007.
[19] P. Dong, W. Qian, S. Liao, H. Liang, C.-C. Kung, N.-N. Feng, R. Shafiiha, J. Fong, D. Feng, A. Krishnamoorthy, and M. Asghari, "Low loss shallow-ridge silicon waveguides," *Opt. Express*, vol. 18, no. 14, pp. 14 474–14 479, Jul. 2010.
[20] F. Utreras, "Natural spline functions, their associated eigenvalue problem," *Numerische Mathematik*, vol. 42, no. 1, pp. 107–117, Mar. 1983, DOI:10.1007/BF01400921. [Online]. Available: http://dx.doi.org/10.1007/BF01400921
[21] G. Farin, *Curves and Surfaces for Computer-Aided Geometric Design*. New York: Elsevier Sci. Technol., 1997.
[22] H. Phien and N. Dejdumrong, "Efficient algorithms for Bézier curves," *Comput. Aided Geom. Design*, vol. 17, no. 3, pp. 247–250, Mar. 2000.
[23] *The IPKISS Parametric Design Framework*. [Online]. Available: www.ipkiss.org
[24] P. Bienstman, L. Vanholme, W. Bogaerts, P. Dumon, and P. Vandersteegen, "Python in nanophotonics research," *Comput. Sci. Eng.*, vol. 9, no. 3, pp. 2801–2803, 2007.
[25] W. Bogaerts, D. Taillaert, B. Luyssaert, P. Dumon, J. Van Campenhout, P. Bienstman, D. Van Thourhout, R. Baets, V. Wiaux, and S. Beckx, "Basic structures for photonic integrated circuits in Silicon-on-insulator," *Opt. Express*, vol. 12, no. 8, pp. 1583–1591, Apr. 2004.
[26] D. Taillaert, W. Bogaerts, P. Bienstman, T. Krauss, P. Van Daele, I. Moerman, S. Verstuyft, K. De Mesel, and R. Baets, "An out-of-plane grating coupler for efficient butt-coupling between compact planar waveguides and single-mode fibers," *J. Quantum Electron.*, vol. 38, no. 7, pp. 949–955, Jul. 2002.
[27] W. Bogaerts, P. Dumon, D. Van Thourhout, and R. Baets, "Low-loss, low-crosstalk crossings for SOI nanophotonic waveguides," *Opt. Lett.*, vol. 32, no. 19, pp. 2801–2803, Oct. 2007.